Jurnal Ilmu Fisika
Vol. 14, No. 2, September 2022, pp. 73–85
ISSN: 1979-4657 (Print); 2614-7386 (Online)
https://doi.org/10.25077/jif.14.2.73-85.2022

Jurnal Ilmu Fisika
Open Access

Comparison of Deformation Vectors Due to Earthquake in Subduction Zone and Sumatran Fault for Each Phase of Earthquake Cycle

Fadilla Monica[1], Vira Friska[1], Deasy Arisa[2], Marzuki Marzuki[1]
[1] Department of Physics, Faculty of Mathematics and Natural Sciences, Universitas Andalas, Pauh, Padang 25163, Indonesia.
[2] Research Center for Geological Disaster, National Research and Innovation Agency, Bandung 40135, Indonesia

Article Info

Article History:

Received April 10, 2022
Revised June 07, 2022
Accepted June 10, 2022

Keywords:

deformation vector
InaCORS
SuGAr
Sumatra
earthquake

Corresponding Author:

Marzuki Marzuki,
Email: marzuki@sci.unand.ac.id

ABSTRACT

This study compares the deformation in West Sumatra due to the earthquakes in the subduction zone and the Sumatran Fault. The Mw6.0 Mentawai earthquake 2019 with a thrust fault mechanism and the Mw5.4 South Solok earthquake 2019 with a strike-slip fault mechanism were used as case studies for the subduction zone and Sumatran Fault, respectively. The deformation was observed using 12 SuGAr (Sumatra GPS Array) and 8 InaCORS (Indonesian Continuously Operating Reference Station) stations, which were processed using GAMIT/GLOBK software. There are differences in the deformation vectors of the two earthquakes. The Mentawai earthquake experienced larger energy accumulation than the South Solok earthquake. The coseismic phase of the Mentawai earthquake experienced the largest horizontal shift at the SLBU station, which was 15.48 mm in the direction of S29.96W, while the South Solok earthquake is found to horizontally shift the CSDH station at the size of 5.75 mm towards S11.45E. The postseismic phase of the Mentawai earthquake lasted 60 days, longer than the South Solok earthquake (20 days). The difference in deformation characteristic between these two earthquakes found in this study will be valuable information in modeling earthquakes in Sumatra.

1. INTRODUCTION

West Sumatra Province, situated in Indonesia, stands as a region inherently vulnerable to earthquakes. Its seismic activity is attributed to three predominant earthquake-generating sources, tied to the interplay between the Eurasian Plate and the India-Australia Plate (refer to Figure 1). These seismic sources encompass the subduction zone (megathrust), the Mentawai (backthrust) Fault, and the widely recognized Sumatran (strike-slip) Fault, often referred to as the Semangko Fault or the great Sumatran Fault (Sieh & Natawidjaja, 2000; Alif et al., 2020).

This subduction zone owes its existence to the movement of the Indian-Australian Ocean Plate, which slides beneath the Eurasian continental plate at an average rate of 60-70 mm/yr (Prawirodirdjo et al., 2000). Historically, the Sumatran subduction zone has been an epicenter for significant seismic activity, with notable events like the Mw8.9 earthquake in 1833 near the Siberut segment and the Mw8.3–Mw8.7 in 1797 (Scholl et al., 2015). Furthermore, recent times have witnessed major tremors in this zone, including the Mw8.7 Nias-Simeulue earthquake in 2005 and the catastrophic Mw9.2 Sumatra-Andaman earthquake in 2004, which was followed by a devastating tsunami.

Positioned centrally in the subduction pathway, the Mentawai Fault moves with a velocity of 5 mm/yr (Tong et al., 2018) and is identified as a backthrust with a southwesterly inclination, showing no signs of strike-slip motion (Sieh & Natawidjaja, 2000). Seismic activities attributed to this fault have

led to events like the Mw8.4 Bengkulu earthquake in 2007 and the Mw7.7 Pagai earthquake in 2010, the latter causing a 7-meter tsunami on Pagai Island.

The Sumatran Fault, characterized by its horizontal orientation and dextral strike-slip mechanism, spans over 1900 km along mainland Sumatra. Comprising 19 primary segments, seven of these segments play a crucial role in determining West Sumatra's seismicity, historically producing earthquakes of magnitude greater than 7 (as cited by Sieh & Natawidjaja, 2000).

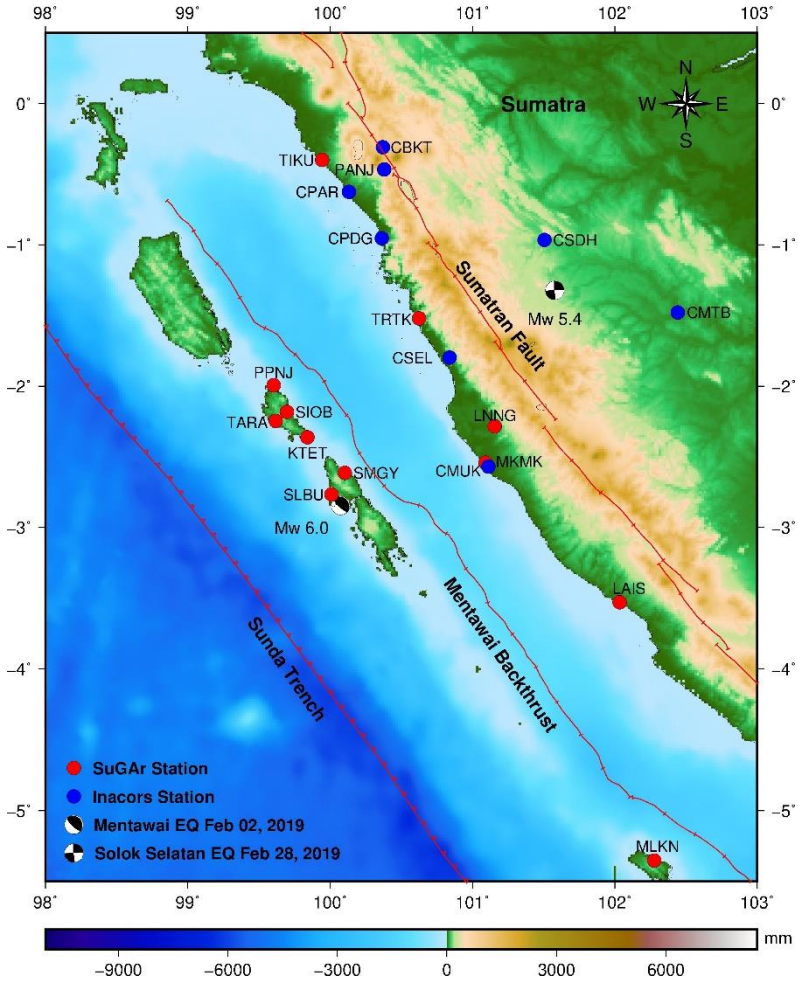

Figure 1 Distribution of SuGAr and InaCORS stations and the epicenter of the 2019 Mentawai and South Solok (Solok Selatan) earthquakes.

Earthquakes induce both vertical and horizontal deformations in the earth's crust. Such deformation, a manifestation of geodynamic processes, results from abrupt shifts like earthquakes or similar seismic events, reflecting the energy distribution and destruction they cause (Krasnoperov, 2009). Consequently, it's pivotal to map these deformation patterns to comprehend the energy distribution of earthquakes and their subsequent impacts.

A primary technique to observe these deformations utilizes geodetic GPS, wherein observation stations are strategically positioned in earthquake-prone areas. Sumatra, for instance, has long benefitted from continuous GPS surveillance through networks like SuGAr (Sumatran GPS Array) and InaCORS, managed by the National Research and Innovation Agency (BRIN) and the Geospatial Information Agency (BIG) respectively (McLoughlin et al., 2011; Aditiya et al., 2014; Masykur, 2021). This surveillance is invaluable in delineating the conditions of observation points throughout the entire earthquake cycle, encompassing the interseismic (energy accumulation between two quakes), preseismic (just before an earthquake), coseismic (during the quake), and postseismic (energy release post-quake) phases (Catherine & Gahalaut, 2007; Govers et al., 2018).

Several research initiatives have employed continuous GPS data to explore the coseismic and postseismic phases. For example, Qiu et al. (2019) employed almost a decade's worth of data post the Mw8.7 Nias-Simeulue earthquake in 2005, revealing a significant 0.22 m southwestward shift due to the quake. Moreover, Sinaga et al. (2020) observed that mainland Sumatra experienced notable coseismic deformation due to subduction, with a notable shift at the NIAN station in Nias. Another study by Effendi et al. (2018) highlighted the shift resulting from the Sianok earthquake in 2007, ranging between 19.0 mm to 135.4 mm.

It's worth noting that while mechanisms differ between subduction zone and Sumatran fault earthquakes, they aren't isolated. Initial studies by Rifai and Pudja (2010) discovered a correlation: seismic events in the subduction zone often preempt quakes on the mainland. Their findings, however, were restricted to examining individual earthquake sources. This study, therefore, aims to concurrently contrast deformations from both the subduction zone and the Sumatran Fault across preseismic, coseismic, and postseismic phases. Building on prior research (Friska et al., 2022; Marzuki et al., 2022; Monica et al., 2022), we scrutinized two 2019 earthquakes: the Mw6.0 Mentawai and the Mw5.4 South Solok, detailing their impacts, epicenters, and consequences. With data sourced from the SuGAr and InaCORS networks and processed via the GAMIT/GLOBK software, our results delve into the comparative deformation vectors and mechanisms of these quakes, offering insights pivotal for disaster mitigation strategies by elucidating the energy release durations inherent to seismic activities.

2. METHOD

This research was conducted using a geodetic approach based on position change before, during, and after the earthquakes using continuous GPS observation data.

Table 1 Locations of SuGAr and InaCORS stations.

Stations	Location	Latitude	Longitude
SuGAr			
KTET	Katiet. Sipora. Kepulauan Mentawai	-2.362540	99.840700
LAIS	Lais. Bengkulu	-3.529130	102.034000
LNNG	Lunang. Bengkulu	-2.285310	101.156000
MKMK	Bandara Muko Muko. Bengkulu	-2.542640	101.091000
MLKN	Malakoni. Pulau Enggano	-5.352670	102.277000
PPNJ	Pulau Siburu. tua pejat	-1.994000	99.603700
SIOB	Sioban. Kepulauan Mentawai	-2.182710	99.696400
SLBU	Silabu. Pagai Utara. Kepulauan Mentawai	-2.766403	100.009720
SMGY	Saumanganya. Pagai Utara. Kep. Mentawai	-2.614490	100.103000
TARA	Taraet. Kepulauan Mentawai	-2.246840	99.617700
TIKU	Tiku. Sumatera Barat	-0.399110	99.944200
TRTK	Taratak. Bengkulu Utara	-1.520750	100.624167
InaCORS			
CBKT	Bukittinggi. Sumatera Barat	-0.3089	100.3711
CMTB	Muara Tebo. Jambi	-1.4791	102.4415
CMUK	Muko-Muko. Bengkulu	-2.5701	101.1120
CPAR	Pariaman. Sumatera Barat	-0.6250	100.1320
CPDG	Padang. Sumatera Barat	-0.9540	100.3631
CSEL	Balai Selasa. pesisir Selatan	-1.7981	100.8391
PANJ	Padang Panjang. Sumatera Barat	-0.4663	100.3795
CSDH	Sungaidareh. Dhamasraya	-0.9661	101.5062

2.1 Data

2.1.1 SuGAr and InaCORS Data

SuGAr stations are spread along the west coast of Sumatra with a total number of 58 stations (Iqbal et al., 2021). The station selection was carried out by taking into account the station data's completeness and position concerning the epicenter of the earthquake. There are 12 SuGAr stations used in this study, and among six of them are closest to the epicenter of the Mentawai earthquake that occurred on February 2, 2019. The other six SuGAr stations are located on mainland Sumatra (see Figure 1 for the distribution of these stations).

The observation for the South Solok earthquake used more data from the InaCORS stations in mainland Sumatra compared to the SuGAr networks due to the limited observation stations of SuGAr in the mainland. This study used six InaCORS stations in West Sumatra and two InaCORS stations in Jambi and Bengkulu. The locations and coordinates of these stations can be found in Figure 1 and Table 1.

2.1.2 IGS Data

IGS or International GNSS Service stations are used as tie-in points which are first selected based on their locations. The 16 selected IGS stations represent the plates surrounding the observed area (as shown in Figure 2).

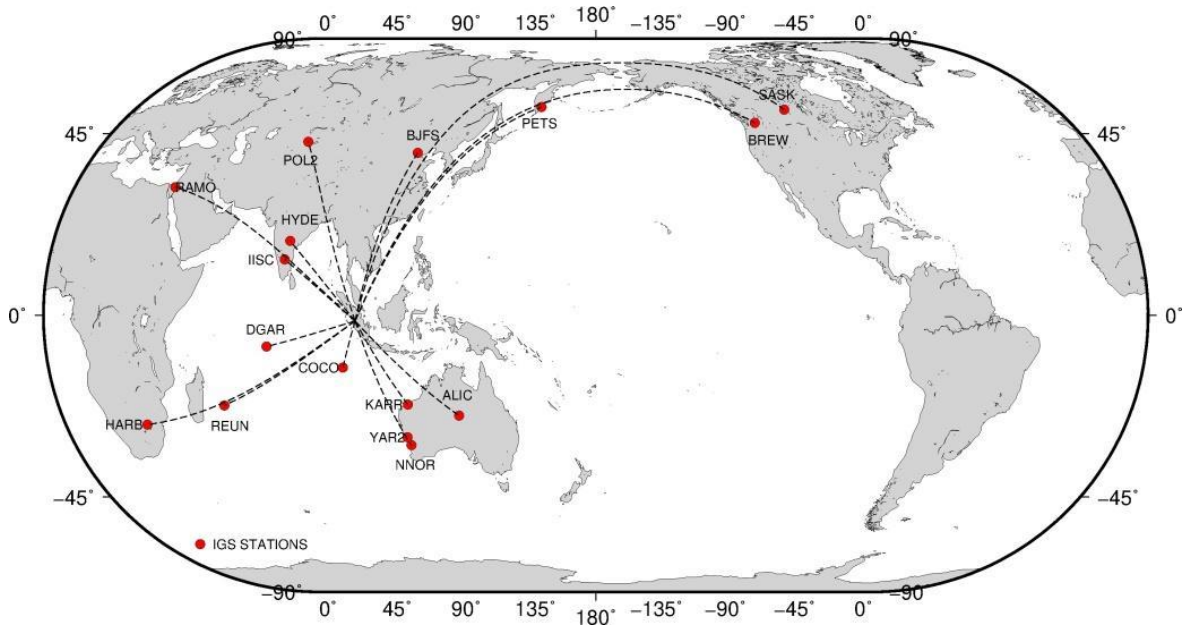

Figure 2 Distribution of IGS stations used in this study.

2.2 Data Processing

Observation data in RINEX format from GPS stations were processed using the GAMIT/GLOBK software (version 10.74) and all resulted figures are plotted using the GMT software.

2.2.1 Data processing with GAMIT software

GAMIT (GPS Analysis Massachusetts Institute of Technology) is a comprehensive, fully automatic processing scientific software for automatic GPS data analysis, developed by the Massachusetts Institute of Technology (MIT) (Herring et al., 2010). GAMIT processing estimates the station coordinates to represent deformation during seismic activity. In its processing, GAMIT requires eight kinds of input data, including: raw data, l-file, station.info, session.info, navigation, sestbl, sittbl, and GPS ephemeris file. The final result of processing GPS observation data with GAMIT is h-files, q-files, and autcl.summary file.

2.2.2 Data processing with GLOBK software

GLOBK (Global Kalman filter VLBI and GPS analysis program) is a program package to perform analysis and further processing after GAMIT processing. The h-files from GAMIT are required as an input file in GLOBK processing. This results in the daily position data in topocentric coordinates (north, east, up) and geocentric coordinates (*X*, *Y*, *Z*). In addition, a time series graphic is also generated, equipped with an error bar that shows the movement of the station (Herring et al., 2010).

2.2.3 Mapping with GMT (Generic Mapping Tools)

The shift vector from GPS observation data was projected into a graphic using the GMT 5.4.5 software (Generic Mapping Tools) (Wessel & Smith, 1999). The GLOBK output, daily position in topocentric coordinates (N, E), and deformation velocity (V_e and V_n) for both networks, are further used in the analysis, graphic, and map plot.

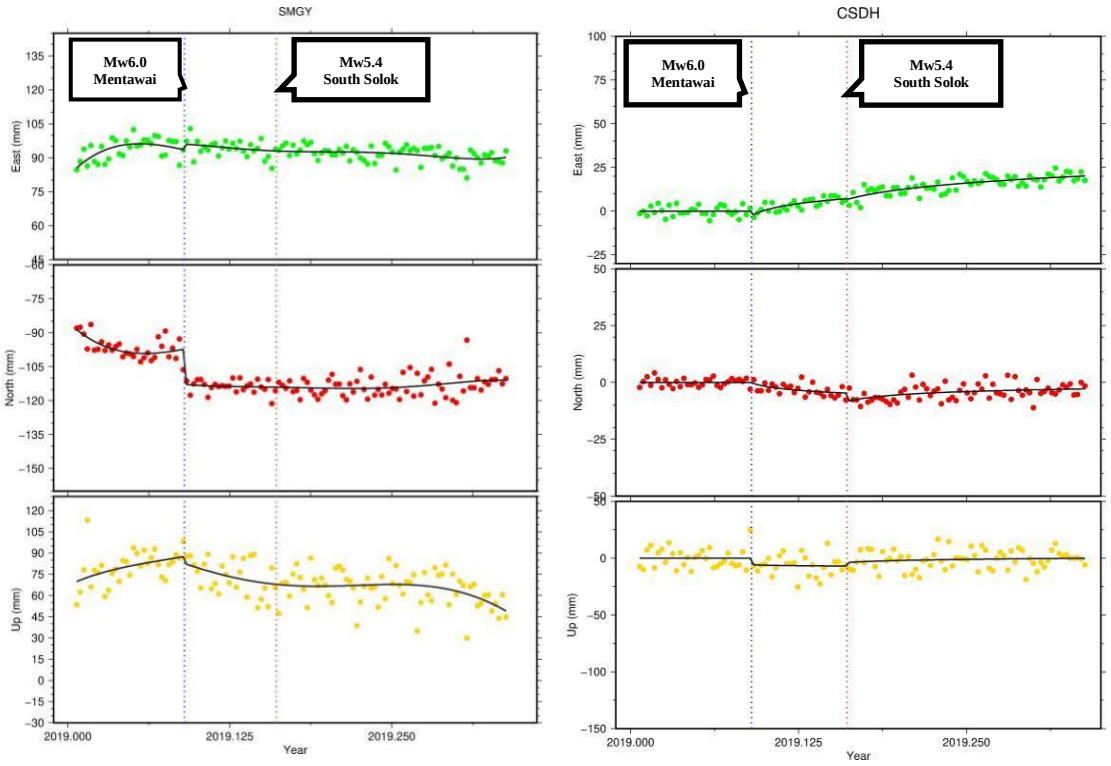

Figure 3 Time series from fault deformation at SMGY (a) and CSDH (b) stations. The dotted vertical line indicates the coseismic jump at Day-Of-Year 033 (Mentawai earthquake) and Day-Of-Year 059 (South Solok earthquake).

2.2.4 Comparative analysis of deformation vector

The comparison of the deformation vector is carried out by looking at the magnitude and direction of the deformation in the coseismic phase, the velocity in the preseismic phase and the velocity in the postseismic phase due to earthquakes that occur based on different mechanisms. The mechanism is a strike-slip fault in the Sumatran fault due to the 2019 South Solok earthquake and thrust faults in the Subduction zone due to the 2019 Mentawai earthquake.

3. RESULTS AND DISCUSSION

3.1 Time Series from the Continuous GPS Observations

The time series of 125 days of GPS observation can be seen in Figure 3, during the time interval from 1 January 2019 (Day-Of-Year (DoY) 001) to 5 May 2019 (DoY 125). The x-axis indicates the observation day, and the y-axis represents the change in position in eastward, northward, and vertical directions, shown as green, red, and yellow graphs, respectively. The day of the Mentawai earthquake (DoY 033) is marked with a light blue dashed vertical line and the South Solok earthquake (DoY 059) is marked with the pink dashed vertical line. The coseismic jump on the Mentawai earthquake can be clearly seen in Figure 3(a) at the SMGY station, which is located at the closest point (approximately 11.4 km) from the epicenter. Meanwhile, the coseismic jump of the South Solok earthquake can be clearly seen in Figure 3(b) at the CSDH station, which is located 30 km from the epicenter. Both earthquakes caused a significant change in the direction of movement before and after the earthquake. The observation in SMGY showed a southwestward movement during the earthquake (it moved northeastward at the interseismic phase), while CSDH showed a southeastward movement during the earthquake (it moved southwestward at the interseismic phase).

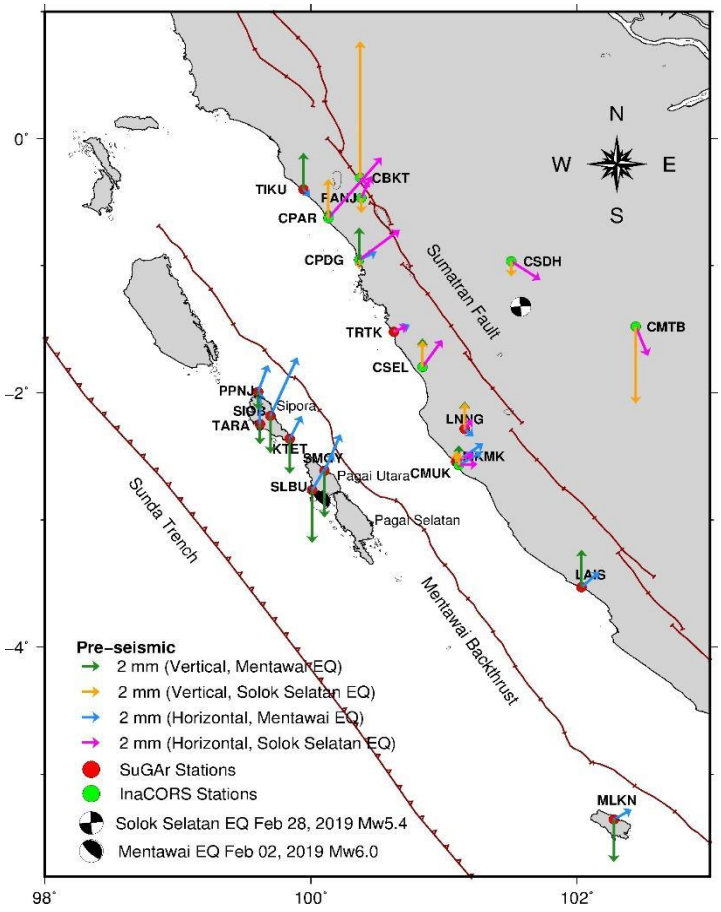

Figure 4 Comparison of the velocity of observation stations in the preseismic phase of the 2019 Mentawai earthquake and the 2019 South Solok (Solok Selatan) earthquake.

3.2 Comparative Analysis of the Deformation of the Mentawai Earthquake and the South Solok Earthquake

3.2.1 Comparison of Deformation during Preseismic Phase

The difference in the direction and size of horizontal and vertical deformation during the preseismic phase was observed from DoY 002 to DoY 032 for the Mentawai earthquake and from DoY 002 to DoY 058 for the South Solok earthquake (Figure 4). In the preseismic phase of the Mentawai

earthquake, most observation stations moved towards the northeast, consistent with the direction of the subduction of the Indo-Australian Plate against the Eurasian Plate (Wang et al., 2022), with the greatest concentration of energy accumulation seen on the island of North Pagai. The SLBU and SMGY stations located in North Pagai have the largest velocity of 4.97 mm/month with a movement direction of N29.40E for SLBU stations and 4.69 mm/month with a movement direction of N22.85E for SMGY stations. Meanwhile, in the preseismic phase of the South Solok earthquake, the eastern part of Sumatran fault moved southeastward, and the western part moved northeastward, meaning that the Indo-Australian Plate movement is still influencing the western part of Sumatra. During the preseismic phase, the CSDH station at the east of the Sumatra Fault moved at the velocity of 3.97 mm/month and the CMTB station moved at the velocity of 3.73 mm/month.

The vertical velocity at stations in the Mentawai Islands has a negative value at a rate of 1.26 - 6.26 mm/month, indicating that these area are experiencing subsidence. The subsidence is in accordance with the results of the morphological analysis of microatoll corals, which concluded that the Mentawai Islands returned to the energy accumulation phase after the 1797 and 1833 earthquakes, indicated by a subsidence at the rate of 10-15 mm/yr (Natawidjaja et al., 2007). On the other hand, stations located on the western part of Sumatra island are relatively uplifted, which is indicated by a positive vertical velocity at a rate of 0.24 - 4.44 mm/month. This is due to effect of the subduction of the Indo-Australian Plate to the geomorphology of Sumatra, which caused uplifting at the western part of Sumatra and subsidence at the other eastern part (Sieh & Natawidjaja, 2000). The deformation vector of the preseismic phase of the Mentawai earthquake is larger than that of the South Solok earthquake. The deformation velocity and direction during the preseismic phase of the Mentawai earthquake can be seen in Table 2.

Table 2 Comparison of the deformation velocity during preseismic phase of the Mentawai earthquake and the South Solok earthquake.

No	Stations	Mentawai EQ			South Solok EQ		
		Deformation (mm/month)		Shift direction (°)	Deformation (mm/month)		Shift direction (°)
		Horizontal	Vertical		Horizontal	Vertical	
1	KTET	3.03	-4.13	N26.65E	-	-	-
2	LAIS	2.73	4.44	N47.97E	-	-	-
3	LNNG	1.32	3.24	S48.69E	1.41	3.11	N38.09E
4	MKMK	2.77	0.15	N51.15E	2.33	1.15	N64.24E
5	MLKN	2.33	-5.04	N59.58E	-	-	-
6	PPNJ	3.39	-2.12	N19.67E	-	-	-
7	SIOB	3.84	-4.41	N23.82E	-	-	-
8	SLBU	4.97	-6.26	N29.40E	-	-	-
9	SMGY	4.69	-5.54	N22.85E	-	-	-
10	TARA	3.75	-2.37	N0.46E	-	-	-
11	TIKU	1.11	4.32	S39.54E	-	-	-
12	TRTK	1.97	0.24	N65.39E	1.69	16.25	N65.11E
13	CBKT	-	-	-	1.55	-9.14	S45.00E
14	CMTB	-	-	-	3.73	1.49	S22.17E
15	CMUK	3.05	2.35	N59.23E	2.34	4.64	N86.19E
16	CPAR	0.94	1.11	N38.95E	6.53	-1.05	N40.23E
17	CPDG	2.20	3.83	N64.13E	5.83	-1.78	N52.46E
18	CSDH	-	-	-	3.97	3.12	S56.39E
19	CSEL	2.11	3.39	N32.41E	3.91	16.25	N35.03E
20	PANJ	-	-	-	2.82	-1.76	N23.84E

3.2.2 Comparison of Deformation during Coseismic Phase

Figure 5 shows the comparison deformation velocity and direction during the coseismic phase of Mentawai earthquake and South Solok earthquake. Several stations experienced changes in the direction of plate deformation from the inter- and preseismic period of the Mentawai earthquake where the stations in the Mentawai Islands tend to move southwestward. The factor that causes changes in the direction of deformation is the elastic nature of the rock in the subduction zone from the trough to a depth of 40 km. (Simoes et al., 2004). Based on the earthquake data from the USGS, this earthquake occurred at a depth of 20 km, which indicates that the rock is still elastic, so if it gets very large energy, deformation will occur in the rock (Susilo et al., 2016). The largest horizontal movement in the coseismic phase of the Mentawai earthquake is at the rate of 15.48 mm at SLBU station with a direction of S29.96W and at the rate of 14.73 mm at SMGY station with a direction of S18.85W. Meanwhile, TIKU, MLKN, LAIS, CPAR, CSEL, and CPDG stations experienced the smallest horizontal movement between 1.13 mm - 2.84 mm and had the same direction as before the earthquake to the northeast. Thus, the TIKU, MLKN, and LAIS stations did not experience any coseismic effects from the Mentawai earthquake.

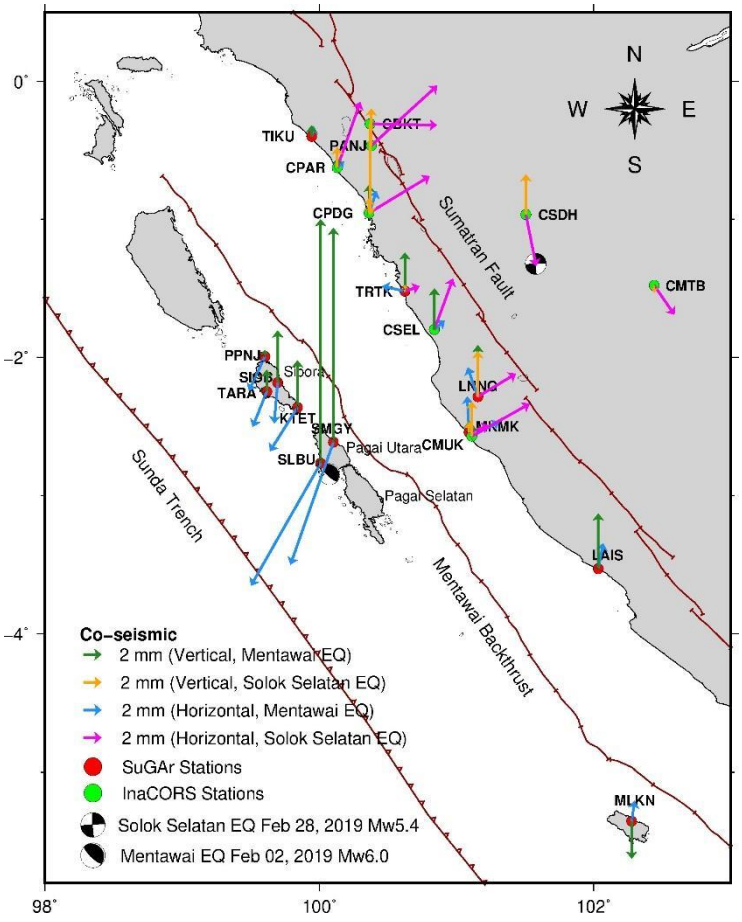

Figure 5 Comparison of the velocity of observation stations in the coseismic phase of the 2019 Mentawai earthquake and the 2019 South Solok (Solok Selatan) earthquake.

The Mentawai earthquake is classified as a shallow earthquake caused by the subduction activity of the Indo-Australian Plate under the Eurasian Plate (Haridhi et al., 2018), at the Pagai segment. A thrust fault triggered this earthquake-generating source. Thrust faults are plate faults that move up with fault plane dips of 45º (Susilo et al., 2016). This causes the observation station in the coseismic phase to experience horizontal and vertical movements. The vertical movement is seen as a positive trend in the time series SuGAr stations (see Table 3). This positive trend was significantly seen at the stations in the Mentawai Islands, especially at SLBU (26.75 mm) and SMGY (23.50 mm). Paleogeodetic coral

studies research also shows that during the 1797 and 1833 earthquakes, the Mentawai Islands experienced a 2-3 m uplift, and the 2007 megathrust earthquake (Mw8.4) also lifted the west coast of South Pagai Island about 1 m (Natawidjaja et al., 2007).

The South Solok earthquake was triggered by seismic activity originating from the large Sumatran Fault, with the epicenter between the Suliti and Siulak segments. The Suliti-Siulak segment is part of the Sumatran Fault, which passes through the southern part of West Sumatra Province with a movement velocity at the rate of 10-14 mm/yr with a direction S3.09E (Rahayu et al., 2020). The coseismic deformation on this fault has a very damaging effect because this fault line is close to residential areas and mostly produces shallow crustal earthquakes. The horizontal movement seen at CSDH station, the closest station to the earthquake epicenter, is 5.75 mm. The movement trends before the earthquake was S56.39E and changed toward S11.45E. The CMUK, CSEL, CPDG, CPAR and PANJ stations in the western part of Sumatra experienced a horizontal movement of 5.75 - 9.81 mm, greater than the CSDH station which was closest to the epicenter of the South Solok earthquake. The horizontal movement trend at the CMUK, CSEL, CPDG, CPAR, and PANJ stations is thought to have occurred because these stations were still affected by the postseismic energy of the Mentawai earthquake, which was still lasting on DoY 063. The deformation velocity and direction during the coseismic phase of the Mentawai earthquake can be seen in Table 3.

Table 3 Comparison of the shift vectors of observation stations in the coseismic phase of the 2019 Mentawai earthquake and the 2019 South Solok earthquake.

No	Stations	Mentawai EQ			South Solok EQ		
		Deformation (mm/month)		Shift direction (º)	Deformation (mm/month)		Shift direction (º)
		Horizontal	Vertical		Horizontal	Vertical	
1	KTET	5.68	5.16	S32.49W	-	-	-
2	LAIS	2.84	6.05	N10.95E	-	-	-
3	LNNG	3.39	5.65	N19.67W	2.23	4.99	N59.10E
4	MKMK	3.92	1.22	N2.77W	2.27	1.11	N71.64E
5	MLKN	2.23	-4.11	N8.49E	-	-	-
6	PPNJ	4.16	0.72	S25.21W	-	-	-
7	SIOB	4.47	5.70	S4.88W	-	-	-
8	SLBU	15.48	26.75	S29.96W	-	-	-
9	SMGY	14.73	23.50	S18.85W	-	-	-
10	TARA	4.18	2.37	S21.95W	-	-	-
11	TIKU	1.13	1.20	N12.80E	-	-	-
12	TRTK	2.54	4.23	N77.72W	1.66	0.69	N71.88E
13	CBKT	-	-	-	8.63	-9.96	S8.91E
14	CMTB	-	-	-	3.92	-0.79	S35.03 E
15	CMUK	3.12	1.34	N11.27E	7.32	3.77	N61.16E
16	CPAR	0.96	1.06	N41.63E	7.63	2.22	N19.36E
17	CPDG	2.55	3.07	N71.21E	7.83	1.62	N59.17E
18	CSDH	-	-	-	5.75	4.40	S11.45E
19	CSEL	1.48	4.50	N40.35E	5.93	-0.07	N20.33E
20	PANJ	-	-	-	9.81	4.06	N48.09E

3.2.3 Comparison of Deformation during Postseismic Phase

The postseismic phase of the Mentawai earthquake was calculated the day after the earthquake occurrence (DoY 034 to DoY 125), while the postseismic phase of the South Solok earthquake was observed from DoY 060 to 125. In the postseismic phase of the Mentawai earthquake, the SLBU station had a velocity of 9.17 mm/month, at the direction of S85.62E and the SMGY station had a velocity of

9.49 mm/month towards the S61.82E direction (Table 4). Compared to the phase before the earthquake, these two stations have not shown signs of returning to the energy accumulation period. The deformation velocity becomes smaller because a large amount of energy has been released in the coseismic phase, and the postseismic phase is the period of remaining energy release. The observation area is still experiencing the postseismic phase until 30 days after the Mentawai earthquake. In detail, the deformation velocity is relatively similar to the interseismic period with a little difference in the direction, which means that the postseismic effect due to the Mentawai earthquake still lasted on DoY 063. Meanwhile, the postseismic phase of the Mentawai earthquake ended at DoY 103, which means this phase lasted for 60 days.

Table 4 Comparison of the velocity of observation stations in the postseismic phase of the 2019 Mentawai earthquake and the 2019 South Solok earthquake.

No	Stations	Mentawai EQ			South Solok EQ		
		Deformation (mm/month)		Shift direction	Deformation (mm/month)		Shift direction
		Horizontal	Vertical	(°)	Horizontal	Vertical	(°)
1	KTET	3.79	5.16	S70.75E	-	-	-
2	LAIS	2.28	6.05	N0.25E	-	-	-
3	LNNG	1.24	5.65	N11.31E	2.23	2.23	N37.54E
4	MKMK	2.28	1.22	N0.25E	2.27	2.27	N67.50E
5	MLKN	2.42	-4.11	N63.54E	-	-	-
6	PPNJ	3.14	0.72	N87.80E	-	-	-
7	SIOB	3.23	5.70	S85.57W	-	-	-
8	SLBU	9.17	26.75	S85.62W	-	-	-
9	SMGY	9.49	23.50	S61.82W	-	-	-
10	TARA	3.01	2.37	N26.65E	-	-	-
11	TIKU	1.33	1.20	N40.74E	-	-	-
12	TRTK	1.42	4.23	N18.82E	1.66	1.66	N56.79E
13	CBKT	-	-	-	8.63	1.49	S42.56E
14	CMTB	-	-	-	3.92	2.84	S29.72E
15	CMUK	1.09	1.34	N42.03E	7.32	1.11	N82.81E
16	CPAR	1.67	1.06	N68.52E	7.63	6.44	N33.43E
17	CPDG	2.01	3.07	N38.93E	7.83	4.75	N57.55E
18	CSDH	-	-	-	5.75	2.61	S62.35E
19	CSEL	2.10	4.50	N0.55E	5.93	1.75	N45.70E
20	PANJ	-	-	-	9.81	2.17	N3.95E

In the postseismic phase of the South Solok earthquake, the station to the left of the Sumatra Fault; CMUK, CSEL, CPAR, CPDG, and PANJ, experienced a deformation velocity of 2.34 - 6.53 mm/month, showing almost similar velocity with the pre-earthquake phase (1.11- 6.44 mm/month). The movement direction during the postseismic phase is the same as that of the preseismic phase. CSDH station has a horizontal movement velocity at the rate of 2.61 mm/month, towards the S56.39E direction. The CMTB station has a shift velocity of 2.84 mm/month towards the S29.72E direction. Compared to the phase before the earthquake, these two stations have returned to their energy accumulation phase. In other words, the postseismic effect of the South Solok earthquake ended at DoY 080, meaning that the postseismic phase due to this earthquake only lasted for 20 days. The deformation velocity and direction during the postseismic phase of the Mentawai earthquake can be seen in Table 4. A short duration of postseismic phase has been suggested for other regions (e.g., Perfettini & Avouac, 2014), which is probably due to (i) the retrieved postseismic signal is not well constrained in the long term and (ii) a

small normal stress during the relatively shallow earthquake (Perfettini & Avouac, 2014; Gualandi et al., 2017).

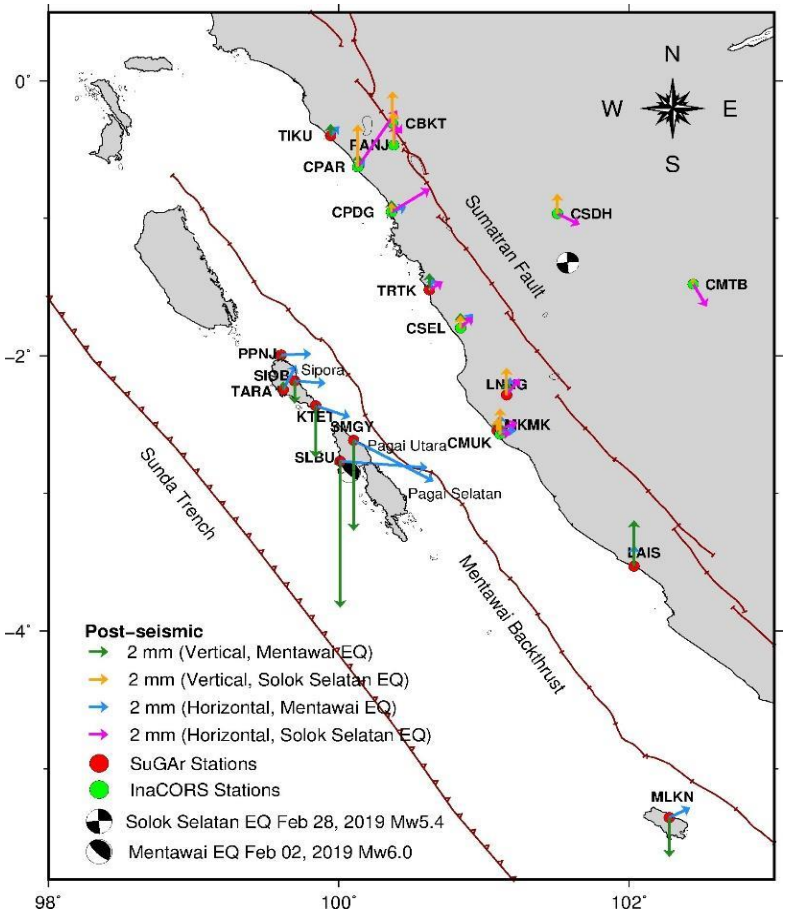

Figure 6 Comparison of the velocity of observation stations in the postseismic phase of the 2019 Mentawai earthquake and the 2019 South Solok (Solok Selatan) earthquake.

4. CONCLUSION

This research set out to compare the deformations resulting from the Mentawai and South Solok earthquakes, seeking to understand their relationship and potential influences on one another within the context of West Sumatra's seismic landscape. Our findings reveal that the Mentawai earthquake on February 2, 2019, did not directly influence the South Solok earthquake on February 28, 2019. This distinction is evident as the impact of the Mentawai quake was localized, predominantly affecting stations near its epicenter, whereas stations proximate to the South Solok quake's epicenter remained unaffected by the Mentawai event.

Stations on the western side of Sumatra primarily registered effects from the thrust fault mechanism of the Mentawai earthquake, in contrast to the dextral strike-slip mechanism of the South Solok event. During the respective seismic phases, the Mentawai earthquake exhibited more pronounced horizontal and vertical displacements compared to the South Solok earthquake. Importantly, the energy from the offshore Mentawai quake was insufficient to induce underwater deformations that could have triggered a tsunami. In contrast, the South Solok earthquake, with its minimal vertical movement, solidified its characterization as a pure strike-slip seismic event.

Furthermore, the postseismic phase duration of the Mentawai earthquake surpassed that of the South Solok earthquake. These specific insights, in conjunction with the broader seismic relationships in Sumatra, emphasize the need for nuanced approaches in earthquake modeling and disaster preparedness in the region.

ACKNOWLEDGMENT

This research was supported by the Professor Acceleration Grant from Andalas University (PDU-KRP2GB-UNAND) (contract no: T/11/UN.16.17/PP.IS-PDU-KRP2GB-Unand/LPPM/2021). Furthermore, thanks to the Center for Geotechnology Research, LIPI, Indonesia, and Nanyang Technological University's Earth Observatory of Singapore for operating the SuGAr network and the Geospatial Information Agency, which operates the InaCORS network.

REFERENCE

Aditiya, A., Efendi, J., & Syafii, A. (2014). InaCORS: Infrastructure of GNSS CORS in Indonesia. *An Article in FIG Congress*, 16–21.

Alif, S. M., Fattah, E. I., & Kholil, M. (2020). Geodetic slip rate and locking depth of east Semangko Fault derived from GPS measurement. *Geodesy and Geodynamics*, 11(3), 222–228.

Catherine, J. K., & Gahalaut, V. K. (2007). A glimpse of earthquake cycle in the Sumatra region. *Current Science*, 92(1), 114–118.

Efendi, J., Prijatna, K., & Meilano, I. (2018). Analysis of the 2007 Sianok Earthquake Coseismic Shift Based on GPS Observation Data in 1993-2007 and the Effect on the 2013 SRGI. *Reka Geomatika*, 2018(1), 1-18.

Friska, V., Arisa, D., Marzuki, M., & Monica, F. (2022). Indo-Australian Plate Velocity Measurement During Interseismic Phase in 2010-2014 Using Sumatran Gps Array (Sugar) Data. *Springer Proceedings in Physics*, Vol. 275, Springer, Singapore.

Govers, R., Furlong, K. P., Van de Wiel, L., Herman, M. W., & Broerse, T. (2018). The geodetic signature of the earthquake cycle at subduction zones: Model constraints on the deep processes. *Reviews of Geophysics*, 56(1), 6–49.

Gualandi, A., Perfettini, H., Radiguet, M., Cotte, N., & Kostoglodov, V. (2017). GPS deformation related to the Mw 7.3, 2014, Papanoa earthquake (Mexico) reveals the aseismic behavior of the Guerrero seismic gap. *Geophysical Research Letters*, 44(12), 6039–6047.

Haridhi, H. A., Huang, B.-S., Kuo-Liang, W., Denzema, D., Prasetyo, R. A., & Chao-Shing, L. (2018). A study of large earthquake sequences in the Sumatra subduction zone and its possible implications. TAO: Terrestrial, *Atmospheric and Oceanic Sciences*, 29(6), 635-652.

Herring, T. A., King, R. W., & McCluskey, S. C. (2010). *Introduction to GAMIT/GLOBK, release 10.4*. Massachusetts Institute of Technology, Cambridge.

Iqbal, R., Arisa, D., & Setiadi, B. (2021). Deformation analysis for Padang earthquake using GPS data. *Journal of Physics: Conference Series*, 1876(1), 12029.

Krasnoperov, R. (2009). Earth crust motion and deformation analysis based on space geodesy methods. Russian *Journal of Earth Sciences*, 11(1), 1–3.

Marzuki, M., Ramadhan, R., Friska, V., Primadona, H., Ramadhan, R. A., Monica, F., Arisa, D., & Namigo, E. L. (2022). Dynamics of West Coast of Sumatra and Island Arc Mentawai during the Coseismic Phase of the Mentawai Mw7.8 25 October 2010 Earthquake. *Journal of Physics: Conference Series*, The 4th International Conference on Research and Learning of Physics (ICRLP 2021) (in press).

Masykur, M. (2021). Analysis of accuracy the InaCORS BIG online post-processing service. *Applied Geomatics*, 13(2), 227–233.

McLoughlin, I. V., Wong, K. J., & Tan, S. L. (2011). Data collection, communications and processing in the Sumatran GPS array (SuGAr). *Proceedings of the World Congress on Engineering*, 2, 6–8.

Monica, F., Arisa, D., Marzuki, M., & Friska, V. (2022). Deformation Analysis During The Pre-, Co- and Post-Seismic Phases Associated with The 2019 Mw6.0 Mentawai Earthquake Using Satellite Geodetic Technology from Sumatran GPS Array (SuGAr) Data. *Springer Proceedings in Physics*, Vol. 275, Springer, Singapore.

Natawidjaja, D.H., Sieh, K., Galetzka, J., & Suwargadi, B.W. (2007). Interseismic deformation above the Sunda Mehathrust recorded in coral microatolls of the Mentawai Islands, West Sumatra. *Journal of Geophysical Research*, 112, 1-27.

Perfettini, H., & Avouac, J. P. (2014). The seismic cycle in the area of the 2011 Mw9. 0 Tohoku-Oki earthquake. *Journal of Geophysical Research: Solid Earth*, 119(5), 4469–4515.

Prawirodirdjo, L., Bock, Y., Genrich, J. F., Puntodewo, S. S. O., Rais, J., Subarya, C., & Sutisna, dan S. (2000). One century of tectonic deformation along the Sumatran fault from triangulation and Global Positioning System surveys. *Journal of Geophysical Research: Solid Earth*, 105(B12), 28343–28361.

Qiu, Q., Feng, L., Hermawan, I., & Hill, E. M. (2019). Coseismic and postseismic slip of the 2005 Mw 8.6 Nias-Simeulue earthquake: Spatial overlap and localized viscoelastic flow. *Journal of Geophysical Research: Solid Earth*, 124(7), 7445–7460.

Rahayu, T., Sinambela, M., Margono, M., Simanullang, A. T., & Ainun, A. R. (2020). *The Tectonic Description of Northern Sumatra*. Yayasan Kita Menulis.

Rifai, L. D., & Pudja, I. P. (2010). Preliminary Study of the Relationship between Continental Earthquakes and Oceanic Earthquakes in Sumatra. *Jurnal Meteorologi Dan Geofisika*, 11(2), 147–153.

Scholl, D. W., Kirby, S. H., von Huene, R., Ryan, H., Wells, R. E., & Geist, E. L. (2015). Great (≥ Mw8. 0) megathrust earthquakes and the subduction of excess sediment and bathymetrically smooth seafloor. *Geosphere*, 11(2), 236–265.

Sieh, K., & Natawidjaja, D. (2000). Neotectonics of the Sumatran fault, Indonesia. *Journal of Geophysical Research: Solid Earth*, 105(B12), 28295–28326.

Simoes, M., Avouac, J. P., Cattin, R., & Henry, P. (2004). The Sumatra subduction zone: A case for a locked fault zone extending into the mantle. *Journal of Geophysical Research: Solid Earth*, 109(B10), 1-16.

Sinaga, S. S., Awaluddin, M., & Sabri, L. M. (2020). Coseismic Deformation Analysis of the Nias Earthquake 3 June 2019 Using CORS BIG and SuGAR data. *Jurnal Geodesi Undip*, 9(4), 12–21.

Susilo, S., Abidin, H. Z., Meilano, I., Prijatna, K., Sapiie, B., Wijanarto, A. B., & Efendi, J. (2016). On the Development of Deformation Model for the Indonesian Geospatial Reference System (IGRS) 2013. *FIG Working Week*.

Tong, X., Sandwell, D. T., & Schmidt, D. A. (2018). Surface creep rate and moment accumulation rate along the Aceh segment of the Sumatran fault from L-band ALOS-1/PALSAR-1 observations. *Geophysical Research Letters*, 45(8), 3404–3412.

Wang, X., Liu, X., Zhao, D., Liu, B., Qiao, Q., Zhao, L., & Wang, X. (2022). Oceanic plate subduction and continental extrusion in Sumatra: Insight from S-wave anisotropic tomography. *Earth and Planetary Science Letters*, 580, 117388.

Wessel, P., & Smith, W. H. F. (1999). *The generic mapping tools (GMT). Technical Reference and Cookbook*, University of Hawaii, USA.